Proceedings of 20th International Congress on Acoustics, ICA 2010

23-27 August 2010, Sydney, Australia

Vibroacoustic Coupling of Cylindrical Structure with Both Excited End Plates

Tsuchiya Hirotarou (1), Kojima Atsushi (1), Moriyama Hiroyuki(2)

Oshinoya Yasuo(2), and Kakimoto Kunihiko (2)

(1) Graduate Shool of Tokai University,Hiratuka,Japan
(2) Tokai University,Hiratuka,Japan

PACS: 43.40.-R

ABSTRACT

Vibroacoustic coupling phenomena occur in a variety of different situations and are generally studied with the goal of controlling noise. However, we also expect that they are applied to new technologies based on energy stored in each system. In this study, we investigate vibroacoustic coupling between structural vibrations and the internal sound fields of thin structures. We consider a cylindrical structure with thin plates at both ends and investigate the coupling between the plate vibrations and the internal sound field when external periodic forces are applied to respective end plates. This coupling is theoretically and experimentally investigated by considering the behavior of the both plates and the acoustic characteristics of the internal sound field with variations in the periodic forces. In the analytical model, the end plates are supported by springs in circumference to make those support conditions close to actual conditions in the experiment due to adjustments of spring stiffnesses, and then the cylinder is assumed to be structurally and acoustically rigid at the lateral wall between the structure and the sound field to simplify this problem. The acoustic characteristics are evaluated by the sound pressure level, which is maximized with changing the phase difference between the both plate vibrations, when the phase difference and relative amplitude between both periodic forces are varied. The behavior of the plate vibration is studied from changing the phase difference with the cylinder length. In comparison between characteristics of the both systems, it is clarified that vibroacoustic coupling is effective in increasing acoustic energy and the phase difference depends greatly on the acoustic mode, which contributes the formation of the sound field.

INTRODUCTION

When structures constructed of plural members vibrate due to an external excitation and so on, neighboring members almost invariably interact with each other, having respective natural modes. Such interactions are caused by energy being transferred between vibration systems. Transfer of vibrational energy occurs not only between vibration systems but also between vibration and acoustic systems; this latter phenomenon is known as vibroacoustic coupling. If a thin structure that encloses a space is excited by an external periodic force, vibroacoustic coupling readily occurs between the structural vibrations and the internal sound field. Pan and Bies investigated a coupled panel–cavity system consisting of a rectangular box with slightly absorbing walls and a simply supported panel as an architectural acoustic problem. They studied the effect of the panel characteristics on the decay behavior of a sound field in the cavity both theoretically and experimentally [1,2]. They concluded that the modal decay times of the system were related to the coupling coefficients, the resonance frequency distribution, the panel modal density, the panel damping and the radiation loss from the panel to the external space. In an attempt to control noise in an airplane, Cheng and Nicolas investigated coupling between the sound field in an aircraft cabin and the vibrations of the rear pressure bulkhead [3,4]. They adopted a cylindrical structure as the analytical model, in which the rear pressure bulkhead at one end of the cylinder was assumed to be a circular plate. This analytical model was examined under a variety of conditions; the plate was supported at its edges by springs, the stiffnesses of which could be adjusted to simulate various support conditions. Their investigations clarified the influence of the support conditions on the sound pressure of an internal sound field coupled with the vibration of the end plate. They also found a frequency range that generates intense sound pressure level.

The results described above are regarded as being important for noise control so that results obtained will be useful for suppressing coupling. On the other hand, such a wave motion into enclosures is also applied to unique technologies, for example a Variable Resonance Induction System (VRIS) is utilized to obtain high torque in all engine speeds [5]. In the VRIS, intake manifolds, which are mounted in each bank of a V-type engine, are connected by resonance tubes. Pressure waves at each cylinder are superposed on each other and cause the resonance corresponding to the dimensions of the manifolds and tubes. The resonance generates high torque characteristics around the resonance frequency, making the pressure in the vicinities of the intake valves and improving the induction process. Since the resonance frequency depends on the dimension of the sound field, the tube's length is varied according to the engine speed. Although the VRIS functions based on the resonance, better improvement is anticipated in induction efficiency on the present VRIS if coupling with the vibrations of the manifolds is taken into consideration.

In the present investigation, we adopt an analytical model similar to the above-mentioned cylindrical structure with plates at both ends, which are excited by point forces. The dimensions of both the plate thickness and the cylinder length are varied because vibroacoustic coupling was estimated by assuming that the plate and cavity dimensions and the phase difference between the vibrations of the two plates were fixed in almost all related investigations. Vibroacoustic coupling is theoretically and experimentally investigated in terms of the vibration and acoustic characteristics. In particular, the phase difference is considered to be a significant characteristic of the vibrations when the sound pressure level and the flexural displacements of the plates are maximized at each cylinder length.

ANALYTICAL METHOD

Equation of plate motion

The analytical model considered herein consists of a cavity with two circular end plates, as shown in Figure 1. The plates are supported by translational and rotational springs distributed at constant intervals and the support conditions are determined by their respective spring stiffnesses T_1 and T_2 and R_1 and R_2, where the suffixes 1 and 2 indicate plates 1 and 2, respectively. The plates having a Young's modulus E and a Poisson's ratio ν change dimensions (i.e., the radius a and the thickness h). The sound field can be assumed to be cylindrical with the same radius as that of the plates and changes the length. The boundary conditions are considered to be structurally and acoustically rigid at the lateral wall between the structure and the sound field. The coordinates used are the radius r, the angle θ between the planes of the plates and the cross-sectional plane of the cavity, and the distance z along the cylinder axis. The periodic point forces F_1 and F_2 are applied to the respective plates at $r_1 = r_2$ and $\theta_1 = \theta_2 = 0$deg.

The flexural displacements w_1 and w_2 on the plates 1 and 2 are expressed by substituting Eq. (2) below for the plate mode shape into Eq. (1) below, and they are expanded over two sets of suitable trial functions:

$$\begin{aligned} w_1 &= \sum_{s=0}^{1}\sum_{n=0}^{\infty}\sum_{m=0}^{\infty} B^s_{1nm} X^s_{nm} \mathrm{e}^{\mathrm{j}(\omega t+\phi_1)} \\ w_2 &= \sum_{s=0}^{1}\sum_{n=0}^{\infty}\sum_{m=0}^{\infty} B^s_{2nm} X^s_{nm} \mathrm{e}^{\mathrm{j}(\omega t+\phi_2)} \end{aligned} \tag{1}$$

$$X^s_{nm} = \sin(n\theta + s\pi/2)(r/a)^m \tag{2}$$

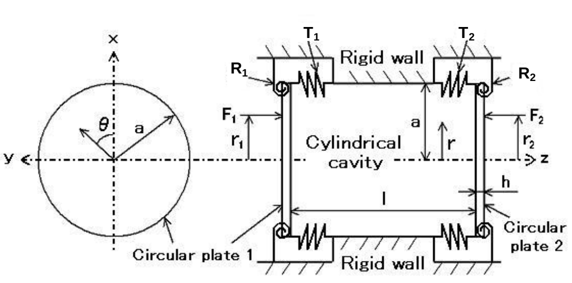

Figure 1. Configuration of the analytical model

where n, m and s are respectively the circumferential order, the radial order and the symmetry index with respect to the plate vibration. $B^s{}_{1nm}$ and $B^s{}_{2nm}$ are the coefficients to be determined, ω is the angular frequency of the periodic point force on the plate and t is the elapsed time. ϕ_1 and ϕ_2 are the phases of the respective plate vibrations; in this analysis, ϕ_1 is set to 0 deg and ϕ_2 varies in the range 0 to 180 deg. The equations of plate motion are obtained by finding the extremum of Hamilton's function in terms of Eq. (1), as follows [3,4]:

$$\left[\sum_{m'=0}^{\infty}\left\{K^s_{1nmm'}\left(1+j\eta_p\right)-\omega^2 M^s_{1nmm'}\right\} + \sum_{m'=0}^{\infty} aF_{sn}\left\{T_1+\left(\frac{m}{a}\right)\left(\frac{m'}{a}\right)R_1\right\}\right]B^s_{1nm'}e^{j\varphi_1} = F^s_{1nm}-P^s_{1nm}, \tag{3}$$

$$\left[\sum_{m'=0}^{\infty}\left\{K^s_{2nmm'}\left(1+j\eta_p\right)-\omega^2 M^s_{2nmm'}\right\} + \sum_{m'=0}^{\infty} aF_{sn}\left\{T_2+\left(\frac{m}{a}\right)\left(\frac{m'}{a}\right)R_2\right\}\right]B^s_{2nm'}e^{j\varphi_2} = -F^s_{2nm}+P^s_{2nm}, \tag{4}$$

where $K^s{}_{1nmm'}$, $K^s{}_{2nmm'}$ and $M^s{}_{1nmm'}$, $M^s{}_{2nmm'}$ are components of the symmetrical stiffness and mass matrices respectively, because the index m' is the radial order ($m = m'$). η_p is the structural damping factor of the plate and F_{sn} is a coefficient that is determined by the indices n and s [3].

The first terms on the right-hand sides of Eqs. (3) and (4) give the point force and the second terms give the acoustic excitation. that also functions as the coupling term between each plate vibration and the sound field. These point force and acoustic excitation terms are, respectively,

$$F^s_{1nm} = \int_{A_1} F_1 \delta(r-r_1)\delta(\theta-\theta_1) X^s_{nm} \mathrm{d}A_1, \tag{5}$$

$$P^s_{1nm} = \int_{A_1} P_c X^s_{nm} \mathrm{d}A_1,\ P^s_{2nm} = \int_{A_2} P_c X^s_{nm} \mathrm{d}A_2. \tag{6}$$

Here, δ is the delta function that represents a point force on the plate, A_1 and A_2 are the areas of both plates and P_c is the sound pressure at an arbitrary position on the boundary surface with the plates.

Coupling equation between plate vibrations and internal sound field

For simplicity, we assume that the cavity walls are rigid, so that the sound field in the cavity is governed by the wave equation consisting of the eigenfunction Y_N and the eigenvalue k_N corresponding to a cavity mode of order N:

$$\nabla^2 Y_N + k_N^2 Y_N = 0 \tag{7}$$

If $\mathbf{u}$ is the unit normal to the boundary surface S (positive toward the outside), the boundary condition satisfies $\partial Y_N/\partial\mathbf{u}$ when S is rigid. However, if S is not rigid but has a specific acoustic admittance that may vary from point to point on the surface, we choose to use a Green's function G to obtain a set of solutions for a non-uniform cavity with non-rigid walls, for a frequency $\omega/2\pi = Kc/2\pi$, where K is an eigenvalue of the non-uniform cavity and c is the speed of sound in the cavity. The equation for G is thus given by

$$\begin{aligned} &\nabla^2 G + K^2 G \\ &\quad = -\delta(p-p_0) = -\delta(r-r_0)\delta(\theta-\theta_0)\delta(z-z_0) \end{aligned} \tag{8}$$

The right-hand side is a delta function, where the measurement point is $\mathbf{p} = (r, \theta, z)$ if the source point is $\mathbf{p}_0 = (r_0, \theta_0, z_0)$. Expressing G with respect to Y_N of Eq. (7) that satisfies the same boundary conditions, we find that

$$G(\mathbf{p}, \mathbf{p}_0) = \sum_{N=1}^{\infty} \frac{Y_N(\mathbf{p}) Y_N(\mathbf{p}_0)}{V_c M_N (k_N^2 - K^2)} \tag{9}$$

$$\int_{V_c} Y_N(\mathbf{p}) Y_M(\mathbf{p}) \mathrm{d}V_c = V_c M_N \delta_{NM} = \begin{cases} 0 \; at \; N \neq M \\ V_c M_N \; at \; N = M \end{cases} \tag{10}$$

The complex dimensionless factor M_N is the mean value of Y_N^2 averaged over the cavity volume V_c and δ_{NM} is the Kronecker delta. Because there is no source and $\partial G/\partial \mathbf{u} = 0$ on S, the spatial factor $P_c(\mathbf{p})$ of the sound pressure within and on the surface bounding the medium can be obtained from just one of the surface integral terms as follows:

$$P_c(\mathbf{p}) = -\int_S G(\mathbf{p}, \mathbf{p}_0) \frac{\partial P_c(\mathbf{p}_0)}{\partial \mathbf{u}_0} \mathrm{d}S_0 \tag{11}$$

where the zero subscripts indicate differentiation and integration with respect to the (r_0, θ_0, z_0) coordinates. A detailed procedure for obtaining these equations is given in Ref. 6. P_c can also be expressed as [3,4]

$$P_c = \rho_c c^2 \sum_{N=1}^{\infty} \frac{P_N Y_N}{M_N} \tag{12}$$

where ρ_c is the fluid density in the cavity and P_N is the pressure coefficient, which is to be determined.

In this investigation, the acoustic modal shape $Y^s{}_{npq}$ and angular resonance frequency ω_{npq} in the cavity (where the indexes n, p and q indicate the circumferential, radial and longitudinal orders, respectively) are defined as

$$Y_{npq}^s = \sin(n\theta + s\pi/2) J_n(\lambda_{np} r) \cos\{(q\pi/L)z\} \tag{13}$$

$$\omega_{npq} = c\left\{\lambda_{np}{}^2 + (q\pi/L)^2\right\}^{1/2} \tag{14}$$

where J_n is the n^{th}-order Bessel function and λ_{np} is the p^{th} solution of an eigenvalue function for a circular sound field having modes (n,p) divided by the radius. The boundary conditions between the plate vibrations and the sound field on the respective plate surfaces are found by assuming continuity of velocities on the plates:

$$\left(\frac{\partial P_c}{\partial \mathbf{u}}\right)_{z=0} = \rho_c \omega^2 w_1, \quad \left(\frac{\partial P_c}{\partial \mathbf{u}}\right)_{z=L} = -\rho_c \omega^2 w_2 \tag{15}$$

where $\partial P_c / \partial \mathbf{u}$ is 0 on the lateral wall of the cylinder since the wall remains rigid. Applying Eq. (15) to Eq. (11), since the analytical mode has two boundary surfaces, P_c becomes

$$P_c = -\int_{A_1} G \rho_c \omega^2 w_1 \mathrm{d}A_1 + \int_{A_2} G \rho_c \omega^2 w_2 \mathrm{d}A_2 \tag{16}$$

On the other hand, by substituting acoustic modes of three orders, n, p and q, instead of the order N of the cavity mode into Eq. (12), P_c can also be expressed as

$$P_c = \rho_c c^2 \sum_{p=1}^{\infty} \sum_{q=0}^{\infty} \frac{P_{npq}^s Y_{npq}^s}{M_{npq}^s} \tag{17}$$

The equation that relates Eqs. (16) and (17) is obtained by applying the Green's function of Eq. (9) to an arbitrary acoustic mode (n,p,q).

$$\left(\omega_{npq}^2 - \omega^2\right) P_{npq}^s = -\frac{\omega^2}{V_c} \left(\int_{A_1} Y_{npq}^s w_1 \mathrm{d}A_1 + \int_{A_2} Y_{npq}^s w_2 \mathrm{d}A_2 \right) \tag{18}$$

where A is the total surface area of the plates. Substituting Eq. (1) for w_1 and w_2 and considering a modal damping factor η_c, Eq. (18) can be rewritten as

$$\begin{aligned} &\left(\omega_{npq}^2 + j\eta_c \omega_{npq} \omega - \omega^2\right) P_{npq}^s \\ &\quad = \frac{A\omega^2}{V_c} \left(-\sum_{m=0}^{\infty} I_1 B_{1nm}^s + \sum_{m=0}^{\infty} I_2 B_{2nm}^s \right) \end{aligned} \tag{19}$$

$$I_1 = \frac{1}{A} \int_{A_1} X_{nm}^s Y_{npq}^s \mathrm{d}A_1, \quad I_2 = \frac{1}{A} \int_{A_2} X_{nm}^s Y_{npq}^s \mathrm{d}A_2 \tag{20}$$

where I_1 and I_2 are the spatial coupling coefficients. Moreover, substituting Eq. (17) for P_c and applying I_1 and I_2 to the integrals in Eq. (6), the acoustic excitation terms $P^s{}_{1nm}$ and $P^s{}_{2nm}$ can be expressed with respect to an arbitrary vibration mode (n,m) as

$$\begin{aligned} P_{1nm}^s &= \rho_c c^2 A \sum_{p=1}^{\infty} \sum_{q=0}^{\infty} \frac{I_1 P_{npq}^s}{M_{npq}^s} \\ P_{2nm}^s &= \rho_c c^2 A \sum_{p=1}^{\infty} \sum_{q=0}^{\infty} \frac{I_2 P_{npq}^s}{M_{npq}^s} \end{aligned} \tag{21}$$

Finally, replacing $P^s{}_{npq}$ in Eq. (21) with those in Eq. (19), and then inserting them in Eqs. (3) and (4), we can complete the coupling equations, whose right-hand sides are as follows:

$$\begin{aligned} &\mathbf{F}_{1nm}^s - \mathbf{P}_{1nm}^s = \mathbf{F}_{1nm}^s \\ &+ \frac{\rho_c c^2 \omega^2 A^2}{V_c} \sum_{m'=0}^{\infty} \sum_{p=1}^{\infty} \sum_{q=0}^{\infty} \frac{I_1 \left(I_1 B_{1nm'}^s e^{j\phi_1} - I_2 B_{2nm'}^s e^{j\phi_2} \right)}{M_{npq}^s \left(\omega_{npq}^2 + \mathrm{j}\eta_c \omega_{npq} \omega - \omega^2 \right)} \end{aligned} \tag{22}$$

$$\begin{aligned} &-\mathbf{F}_{2nm}^s + \mathbf{P}_{2nm}^s = -\mathbf{F}_{2nm}^s \\ &- \frac{\rho_c c^2 \omega^2 A^2}{V_c} \sum_{m'=0}^{\infty} \sum_{p=1}^{\infty} \sum_{q=0}^{\infty} \frac{I_2 \left(I_1 B_{1nm'}^s e^{j\phi_1} - I_2 B_{2nm'}^s e^{j\phi_2} \right)}{M_{npq}^s \left(\omega_{npq}^2 + \mathrm{j}\eta_c \omega_{npq} \omega - \omega^2 \right)} \end{aligned} \tag{23}$$

On the right sides, the second term of Eq. (22) and Eq. (23) show the acoustic excitation for the plates 1 and 2, respectively. The acoustic excitation terms have both I_1 and I_2 since the acoustic mode of the sound field is coupled to the vibration modes of the respective plates. Before the actual calculation, the natural frequency of the plate is always considered in viewpoint of convergence for the plate vibration mode (n,m). In this case, the natural frequency is solved as the eigenvalue of Eq. (3) or (4), whose the right side is set to be 0 due to the assumption of the free vibration. The actual calculation is performed by taking 15 terms for n, while m is set to be greater than 12 to ensure convergence to the natural frequency and to the modal shape of the plate vibration. Employing the same truncation for p as for m, the order accounts for acoustic modes greater than $q = 15$, so that the resonance frequency containing. q includes the excitation frequency. The plate and cavity loss factors are assumed to be constant: $\eta_p = \eta_c = 0.01$ [3,4]. Since $B^s{}_{1nm'}$ and $B^s{}_{2nm'}$ can be obtained from the simultaneous equations in Eqs. (3) and (4), which respectively have Eqs. (22) and (23) as excitation terms, the behavior of the plate vibrations and the sound field under vibroacoustic coupling can be determined.

The sound pressure P_c is obtained from Eq. (17), for which P^s_{npq} is substituted, induced from Eq. (19) employing $B^s_{1nm'}$ and $B^s_{2nm'}$ determined above. The square sound pressure P_v^2 averaged over the entire sound field is defined and the sound pressure level L_{pv} expressed logarithmically relative to $P_0 = 2\times10^{-5}$ Pa as follows:

$$P_v^2 = \frac{1}{2V_c}\int_{V_c} P_c P_c^* \mathrm{d}V_c,\ L_{pv} = 10\log\left(\frac{P_v}{P_0}\right)^2 \tag{24}$$

where P_c* is the conjugate component.

THEORETICAL RESULTS AND DISCUSSION

In this investigation, the plates are assumed to be aluminum having a Young's modulus E of 71 GPa and a Poisson's ratio ν of 0.33 and have a radius a of 150 mm and a thickness h of 2, 3 and 4 mm. The cylindrical sound field having the same radius as that of the plates changes the length in the range 100 to 2000 mm. The support conditions of the plates, which have a flexural rigidity D [= $Eh^3/\{12(1-\nu^2)\}$], are expressed by the non-dimensional stiffness parameters T_n (= T_1a^3/D = T_2a^3/D) and R_n (= R_1a/D = R_2a/D); in the present study, these are identical for both plates. R_n and T_n is 10^8, and hence the support condition is regarded as a clamped support. The natural frequency of the plate corresponding to the (n,m) mode is expressed as f_{nm} and is regarded as the excitation frequency. The only (0,0) mode is employed to simplify this vibroacoustic problem. The point forces F_1 and F_2 are applied to the respective plates at $r_1/a = r_2/a = 0.4$ and their magnitude is represented by the excitation ratio $F_R = F_2/F_1$ due to varying F_2 when F_1 is set to 1 N.The resonance frequency of the cylindrical sound field is represented by f_{npq} (i.e., the natural frequency corresponding to the (n,p,q) mode).

Since acoustic characteristics of the sound field depend on not only F_R but also the respective phases ϕ_1 and ϕ_2, these phases are related by the phase difference ϕ:

$$\phi = \phi_2 - \phi_1 \tag{25}$$

Figure 2 shows changes in the sound pressure level L_{pv} averaged over the entire sound field when the plate of a = 150 mm and h = 3mm is excited by the natural frequency f_{00} = 340 Hz and the cylinder length L is varied between 100 and 2000 mm. The maximized L_{pv} is chosen when ϕ is varied between 0 and 180 deg and is contracted between two ways of the excitation, in which cases exciting one plate and both plates are taken. L_{pv} varies substantially and exhibits peaks in the vicinities of L = 510, 1010 and 1520 mm in both cases. L_{pv} at the excitations of both plates is larger than that at the excitation of one plate in the entire range of L.

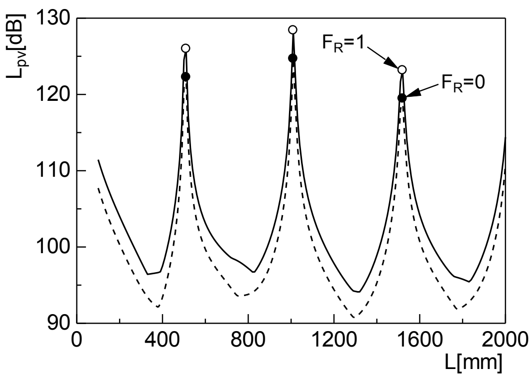

Figure 2. Changes in L_{pv} corresponding to ϕ_{max} with L when one end plate and both end plates of h = 3 mm are excited, respectively

The acoustic mode (0,0,q) causes L_{pv} to have peaks at L = 510, 1010 and 1520 mm, having similar modal shapes to the (0,0) mode of the plate vibrations. These peaks occur at integer q starting from q = 1 with increasing L.

Figures 3(a) and (b) show the variations in L_{pv} when ϕ ranges from 0 to 180 deg; the variations are contrasted in changing F_R and the peaks of L_{pv}, respectively. In Figure 3(a), the variation in L_{pv} is indicated with changing F_R at the principal peak that appeared at L = 510 mm in Figure 2. L_{pv} increases with ϕ and reaches the maximum, which is plotted with circles and occurs in the vicinity of 90 deg when F_R = 0. Here, the values of ϕ at which L_{pv} is a maximum are denoted by ϕ_{max}. Although L_{pv} decreases with increasing ϕ beyond ϕ_{max} and changes similarly despite changing F_R, ϕ_{max} shifts to a lower ϕ and L_{pv} increases gradually with increasing F_R. Figure 3(b) shows the variations in L_{pv} when ϕ not only about the principal peak but also about the second and third peaks that appear L = 1010 and 1520 mm, respectively, when F_R = 1. ϕ_{max} shifts to a lager ϕ than 90 deg at the second peak, shifting to a smaller ϕ than 90 deg at the third peak as well as at the principal peak. As described above, since the order of L_{pv} peaks is identical to the longitudinal order q of the (0,0,q) mode, so that even and odd q makes ϕ_{max} increase and decrease, respectively. In general resonance tube having both closed ends, because the sound pressure at the ends has the opposite signs each other at odd orders, having the same signs each other at even orders, such a shift of ϕ_{max} contributes to intensify the sound field; i.e., it makes L_{pv} peak at L = 510, 1010 and 1520 mm.

The effect of F_R on acoustic characteristics has not been clarified yet, having been estimated from fragmentary results, and so is studied with continuous changes in F_R in Figures 4(a) and (b). Figure 4(a) shows changes in ϕ_{max} with F_R; ϕ_{max} of L = 510 and 1010 mm (i.e., q = 1 and 2) is chosen because $\phi_{\max}$ of q = 1 and 3 almost overlaps each other.

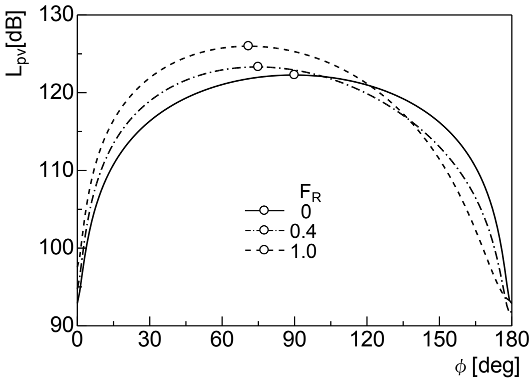

(a) When F_R changes

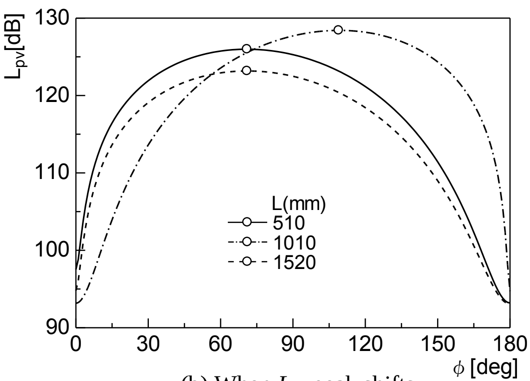

(b) When L_{pv} peak shifts

Figure 3. Variation in L_{pv} with ϕ when h = 3 mm, F_R changes and L_{pv} peak shifts

ϕ_{max} of q = 1 decreases with increasing F_R, being 90 deg at F_R = 0, whereas the decrease is suppressed with increasing F_R and makes ϕ_{max} of q = 1 asymptotic in the proximity of 70 deg. ϕ_{max} of q = 2 has the opposite tendency to that of q = 1 in the increase and decrease and is almost symmetric for that of q = 1 about 90 deg. Figure 4(b) shows changes in L_{pv} with F_R; L_{pv} of L = 510 , 1010 and 1520 mm (i.e., q = 1, 2 and 3) is chosen. L_{pv} increases with F_R in the whole range F_R; the increase becomes proportional over around F_R = 0.4, below which it is suppressed. The range of F_R suppressing changes in L_{pv} reverses as contrasted with that of ϕ_{max}. The value of L_{pv} increases by 3 dB due to applying twice F_1 to the plate, depending also on the magnitude of F_1 according to acoustics. However, L_{pv} of F_R = 1 becomes around 3.7 dB larger than that of F_R = 0. This increase is causes by efficiencies of the energy transfer between the vibration and acoustic systems because of both plate excitations.

Figure 5 shows the changes in ϕ_{max} for both F_R = 0 and 1 to clarify the difference between the one plate excitation and the excitations of both plates. For F_R = 0, ϕ_{max} is about 83 deg at L = 100 mm and it decreases gradually with increasing L up to about L = 380 mm, where it suddenly increases to over 90 deg and subsequently decreases with increasing L.

This behavior of ϕ_{max} is repeated in a similar manner as L increases to L = 2000 mm. The abrupt changes in ϕ_{max} are approximately centered on 90 deg. Such a repeat takes place from shifting the acoustic mode that contributes greatly to the formation of the sound field; the (0,0,1) mode affects the sound field between L = 390 and 740 mm and the nest repeats, which take place between L = 750 and 1290mm and between L = 1300 and1770 mm, are mainly caused by the (0,0,2) and (0,0,3) modes, respectively. ϕ_{max} of F_R = 1 does not change in the regular manner such as that of F_R = 0, whereas it almost changes on the side of in phase in the range of L where the (0,0,1) and (0,0,3) modes affect the sound field at F_R = 0, changing almost on the side of out of phase in the range of L where the (0,0,2) mode affects the sound field at F_R = 0. ϕ_{max} corresponding to the peaks of L_{pv} in Figure 2 is plotted by circles and is close to 90 deg at F_R = 1, being 90 deg at F_R = 0.

EXPERIMENT

Experimental apparatus and method

Figure 6 shows the experimental apparatus used in this investigation. The cylindrical structure consists of a steel cylinder with circular aluminum end plates that are 2, 3 and 4 mm thick. The cylinder has inner diameter of 153 mm and that lengths can be varied from 200 mm to 2000 mm to emulate the analytical model. The periodic point forces excite the end plates of both sides. These forces are applied to the respective plates by small vibrators, the amplitudes of which are controlled to be 1 N. The positions of the point forces r_1 and r_2 are normalized by radius a and they are set to $r_1/a = r_2/a = 0.4$. In this investigation, the main characteristic of the plate vibration under consideration is the phase difference between the plate vibrations. Therefore, acceleration sensors are installed on both plates to measure this phase difference. In order to estimate the internal acoustic characteristics, the sound pressure level in the cavity is measured using a condenser microphone with a probe tube whose tip is located in the vicinity of the plate 2 and the cylinder wall, which is the approximate location of the maximum sound pressure level.

Before conducting the excitation experiment, the natural frequency of the plate is measured by experimental modal analysis using an impulse hammer. It confirmed that the theoretical and experimental natural frequencies are closest when rotational stiffness $R_n = 10^1$; therefore, we can take the experimental support conditions to be translational stiffnesses $T_n = 10^8$ and $R_n = 10^1$.

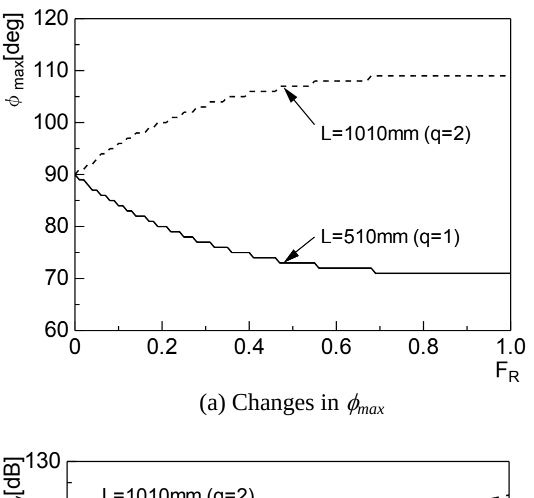

(a) Changes in ϕ_{max}

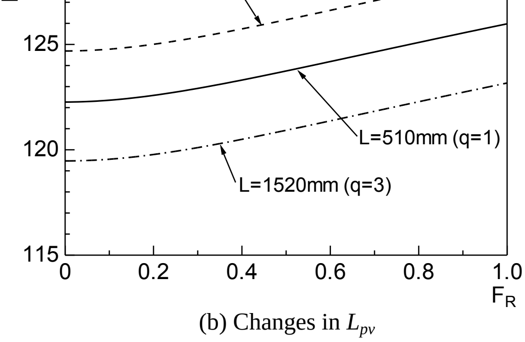

(b) Changes in L_{pv}

Figure 4. Changes in ϕ_{max} and L_{pv} with F_R in each L_{pv} peak when h = 3 mm

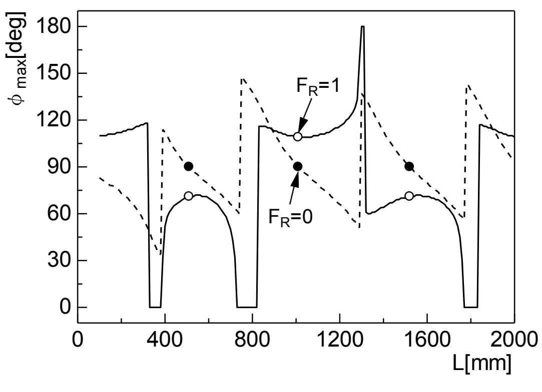

Figure 5. Changes in ϕ_{max} with L when one end plate and both end plates of h = 3 mm are excited, respectively

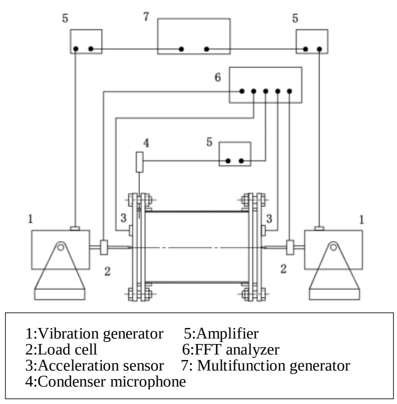

Figure 6. Configuration of the experimental apparatus

Experimental results and discussion

Figure 7 shows changes in the sound pressure level L_{pv} averaged over the entire sound field, corresponding to ϕ_{max} in the analysis, and in the sound pressure level L_p that is measured in the experiment and is maximized when the phase difference between both point forces ranges from 0 deg to 180 deg. Peaks in L_{pv} appear at L = 610, 1230 and 1840 mm; these peaks are known to be caused by the (0,0,1), (0,0,2) and (0,0,3) modes, respectively. L_p increases greatly at 625, 1250 and 1850 mm and peaks at similar values of L to L_{pv}. Figures 8(a) and (b) show changes in L_{pv} and L_p with ϕ; L_{pv} and L_p of the principal and second peaks and in the middle range of their peaks are employed and are the sound pressure level at L = 610, 810, 1230 mm and L = 625, 950, 1250 mm, respectively. In the theoretical results of Figure 8(a), L_{pv} of L = 610 and 1230 mm is maximized in the vicinities of ϕ = 70 and 110 deg; i.e., ϕ_{max} of the principal and second peaks shifts to the sides of in phase and out of phase, respectively, as well as Figure 3(b). Because the acoustic modes dominating over the sound fieldshift with changing L and do not exist in the vicinity of L = 810 mm, L_{pv} remains almost constant for all values of ϕ.

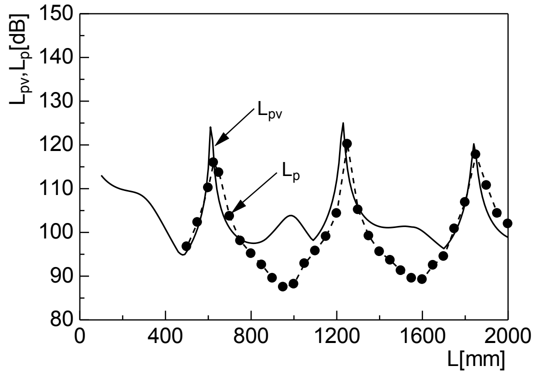

Figure 7. Changes in L_{pv} corresponding to ϕ_{max} and L_p with L when h = 3 mm

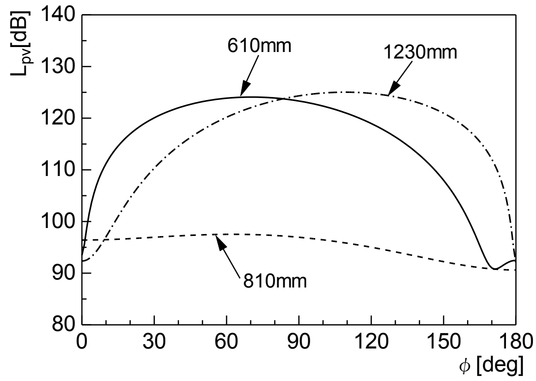

(a) Theoretical results

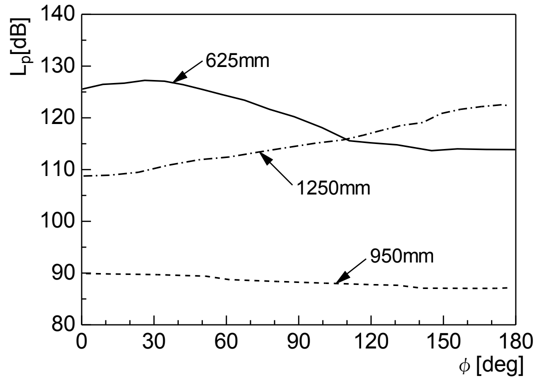

(b) Experimental results

Figure 8. Variations in L_{pv} and L_p with ϕ when h = 3 mm and L changes

Figure 8(b) shows the experimental results L_p corresponding to the above L_{pv}. The appearance of ϕ_{max} is distinguished by shifts to the sides of in phase and out of phase at L = 625 and 1250 mm and L_p is almost constant for all values of ϕ at L = 950 mm. The behavior of L_p supports the justness of the theoretical results, differing from that of L_{pv} near ϕ = 0 and 180 deg.

Since F_R affected greatly the values of L_{pv}, as shown in Figure 4(b), the magnitude of the point forces should be concerned with the flexural displacements w_1 and w_2, and so it is also significant to study the effect of w_1 and w_2 on L_{pv}. In Figure 9, the phase differences are considered when w_1 and w_2 are maximized and are denoted by ϕ_{w1} and ϕ_{w2}, and then the experimental phase difference ϕ_{exp} when L_p is maximized and ϕ_{max} are also indicated when F_R= 0. ϕ_{w1} is constant by 180 deg between L = 100 and 480 mm and decreases abruptly up to 0 deg at L = 490 mm. Remaining constant by 0 deg up to L = 620 mm, ϕ_{w1} increases gradually with L and reaches 180 deg at L = 1240 mm with an increase somewhat promoted in the vicinity of L = 1080 mm. Beyond L = 1240 mm, ϕ_{w1} is constant by 180 deg up to L = 1690 mm again and this behavior is repeated in the same manner as L increases to L = 2000 mm. On the other hand, ϕ_{w2} has gradual and abrupt changes and they are similar to changes in ϕ_{w1}. However, they occur in the alternate range of those of ϕ_{w1} and change the opposite direction to those of ϕ_{w1}; for instance, the gradual decrease occurs between L = 100 and 620 mm and the abrupt increase occurs in the vicinity of L = 1080 mm. ϕ_{w1} and ϕ_{w2} shift between 0 and 180 deg with changing L together and intersect around 90 deg and near the length that L_{pv} peaked in Figure 7. ϕ_{exp} also shift between 0 and 180 deg with changing L and almost corresponds with ϕ_{w1} and ϕ_{w2}, but they are different between L = 900 and 1100 mm and between L = 1550 and 1700 mm. As contrasted with ϕ_{max} of F_R = 0 that changes periodically with shifting the (0,0,q) modes, ϕ_{exp} and ϕ_{max} have good correspondence between the abrupt changes and the shifts of the (0,0,q) modes. Moreover, when L_p peaks at L = 650 and 1850 mm in Figure 7, ϕ_{exp} deviates somewhat from the side of in phase. The small deviations reflect the theoretical results in Figure 5, in which ϕ_{max} was close to 90 deg when L_{pv} peaked at F_R = 1.

In order to justify the above estimation for the vibroacoustic phenomena, the theoretical and experimental results for the plates of h = 2 and 4 mm, whose the natural frequencies are different form that of h = 3 mm, are estimated such as those of h = 3 mm.Figures 10(a) and (b) show changes in the sound pressure levels L_{pv} and L_p and the phase differences ϕ_{w1} ,ϕ_{w2}, ϕ_{exp} and ϕ_{max} with L when h = 4 mm and the theoretical and experimental f_{00} is 375 and 388 Hz, respectively, as well as Figures 7 and 9. L_{pv} and L_p have four peaks between the first and the forth in the vicinities of L = 460, 920, 1370 and 1830 mm caused by the (0,0,1), (0,0,2), (0,0,3) and (0,0,4) modes, respectively. ϕ_{w1} and ϕ_{w2} shift between 0 and 180 deg with changing L and ϕ_{exp} corresponds to them.

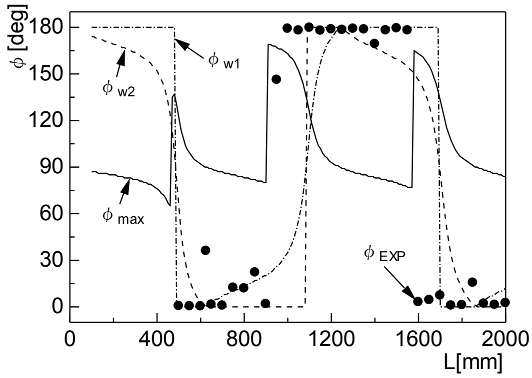

Figure 9. Comparison between ϕ_{w1} ,ϕ_{w2} and ϕ_{exp} for excitations of both ends and ϕ_{max} for one end excitation when h = 3 mm

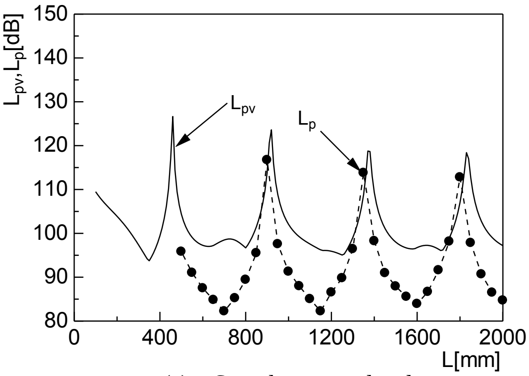

(a) Sound pressure leval

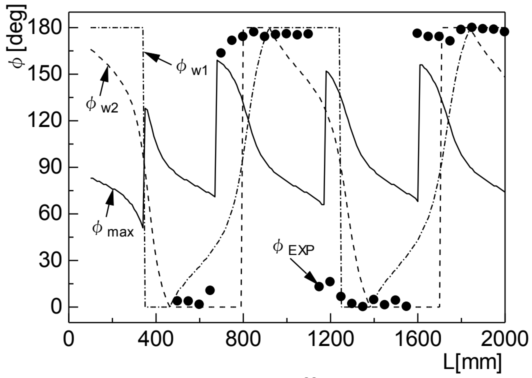

(b) Phase difference

Figure 10. Changes in L_{pv} corresponding to ϕ_{max} and L_p with L and comparison between ϕ_{w1} ,ϕ_{w2} and ϕ_{exp} for excitations of both ends and ϕ_{max} for one end exctation when h = 4 mm

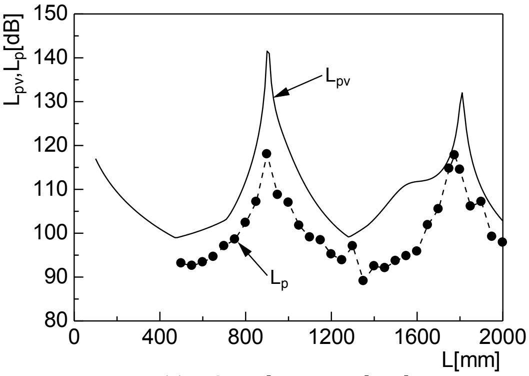

(a) Sound pressure leval

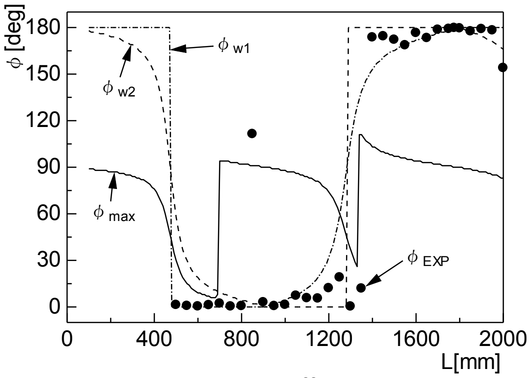

(b) Phase difference

Figure 11. Changes in L_{pv} corresponding to ϕ_{max} and L_p with L and comparison between ϕ_{w1} ,ϕ_{w2} and ϕ_{exp} for excitations of both ends and ϕ_{max} for one end excitation when h = 2 mm

ϕ_{max} also repeats increase and decrease with changing L up to L = 2000 mm and its abrupt changes are almost identical to those of ϕ_{exp}. The natural frequency f_{00} of h = 4 mm is higher than that of h = 3 mm, so that the intervals of L, at which L_{pv} peaks and the dominant acoustic modes shift, are shortened. However, ϕ_{w1} and ϕ_{w2} shift also intersect around 90 deg and near the length that L_{pv} peaks. In case of h = 2 mm, the sound pressure level and the phase difference behave as the similar manner to those of h = 3 and 4 mm, as shown in Figures 11(a) and (b). Since the theoretical and experimental f_{00} of h = 2 mm are, respectively, 190 and 203 Hz and are the lowest in these natural frequencies, so that the interval of L at which L_{pv} peaks is expanded and the dominant acoustic modes shift at the longer L in comparison with the other cases. In particular, ϕ_{exp} at L = 850 mm at which L_p peaks deviates greatly from the side of in phase. If it is considered to decrease the flexural rigidity with h, the flexural displacements of h = 2 mm are larger than those of h = 3 and 4 mm, so that it is thought that the deviation reflects more greatly the theoretical results in Figure 5.

CONCLUSIONS

Vibroacoustic coupling between plate vibrations and a sound field is investigated for a cylindrical structure with circular end plates. Both end plates are excited by periodic point forces, the frequency of which is the natural frequency of the plate. This study focuses on the excitation ratio between both point forces and the phase difference between the vibrations of the two plates in terms of the effect of coupling on the vibration characteristics of the plate.

the theoretical study found that if the excitation ratio ranges from one end excitation to the excitations of both ends by the same point forces, the phase difference shifts from 90 deg to the side of in phase or out of phase when the dominant acoustic mode has the odd or even longitudinal order.The excitations of both ends make the acoustic energy increase efficiently, activating the energy transfer between the vibration and acoustic systems in comparison with one end excitation. If the effect of the phase difference is focused on the flexural displacements of both plates, the respective phase differences that maximize the flexural displacements shift between in phase and out of phase with changing the cylinder length. The experimental phase difference almost corresponds to the theoretical results, being somewhat different from them at shifting the phase difference between in phase and out of phase, and shifts with the dominant acoustic mode.

REFERENCE

1 J. Pan, D.A. Bies, “The effect of fluid-structural coupling on sound waves in an enclosure - theoretical part” *Journal of the Acoustical Society of America* **87** (2), 691-707 (1990)
2 J. Pan, D.A. Bies, “The effect of fluid-structural coupling on sound waves in an enclosure - experimental part” *Journal of the Acoustical Society of America* **87** (2), 708-717 (1990)
3 L. Cheng, J. Nicolas, “Radiation of sound into a cylindrical enclosure from a point-driven end plate with general boundary conditions” *Journal of the Acoustical Society of America* **91** (3), 1504-1513 (1992)
4 L. Cheng, “Fluid-structural coupling of a plate-ended cylindrical shell: vibration and internal sound field” *Journal of Sound and Vibration* **174** (5), 641-654 (1994)
5 K. Hatamura et al., “Mazuda’s new V-6 gasoline engine and its innovative induction system” *SAE Paper*, No. 871977 (1987).
6 P. M. Morse, K. U. Ingard, *Theoretical Acoustics* (McGraw-Hill, New York, 1968) pp. 554-561